CHAPTER 1

INTRODUCTION

1.1 Physical property of TiO_2 [1]

Titanium dioxide (TiO_2) is considered as a semiconductor material, commonly known as titania. Although generally used as a pigment or opacifier, it can also be applied in photocatalysis. Three polymorphs of titanium dioxide exist: anatase, rutile, and brookite. All structures of anatase, rutile, and brookite consist of TiO_6^{2-} octahedral, which produce the overall structure of TiO_2. In this structure each Ti atom is surrounded by six oxygen neighboring at the corners of a slightly distorted octahedral. The three crystalline structures differ by the distortion of each octahedral and by the assembly patterns of the octahedral chains[2]. Anatase has four edges sharing per octahedron but no corner oxygen sharing. The arrangement of these octahedral gives the overall structure of anatase as shown in Figure 1.1 b. In rutile, two edges are shared forming a linear chain. The linear chains are joined to each other by sharing of corner oxygen atom, producing the overall rutile structure as shown in Figure 1.1a as a representative in photocatalysts. The octahedral linkages in brookite are such that three edges are shared per octahedron. It has been envisioned that the joining together of these distorted TiO_6^{2-} octahedral forms the overall structure of brookite as shown in Figure 1.1c. The structural properties of the three types of TiO_2 are listed in Table 1.1

Titanium dioxide is an n-type semiconductor [3] that has a band gap of 3.2 eV for anatase[4], 3.0 eV for rutile [5], and ~3.2 eV for brookite [6]. Anatase is the most

widely investigated photocatalyst due to its strong oxidative properties, low cost, non toxicity, chemical and thermal stability.

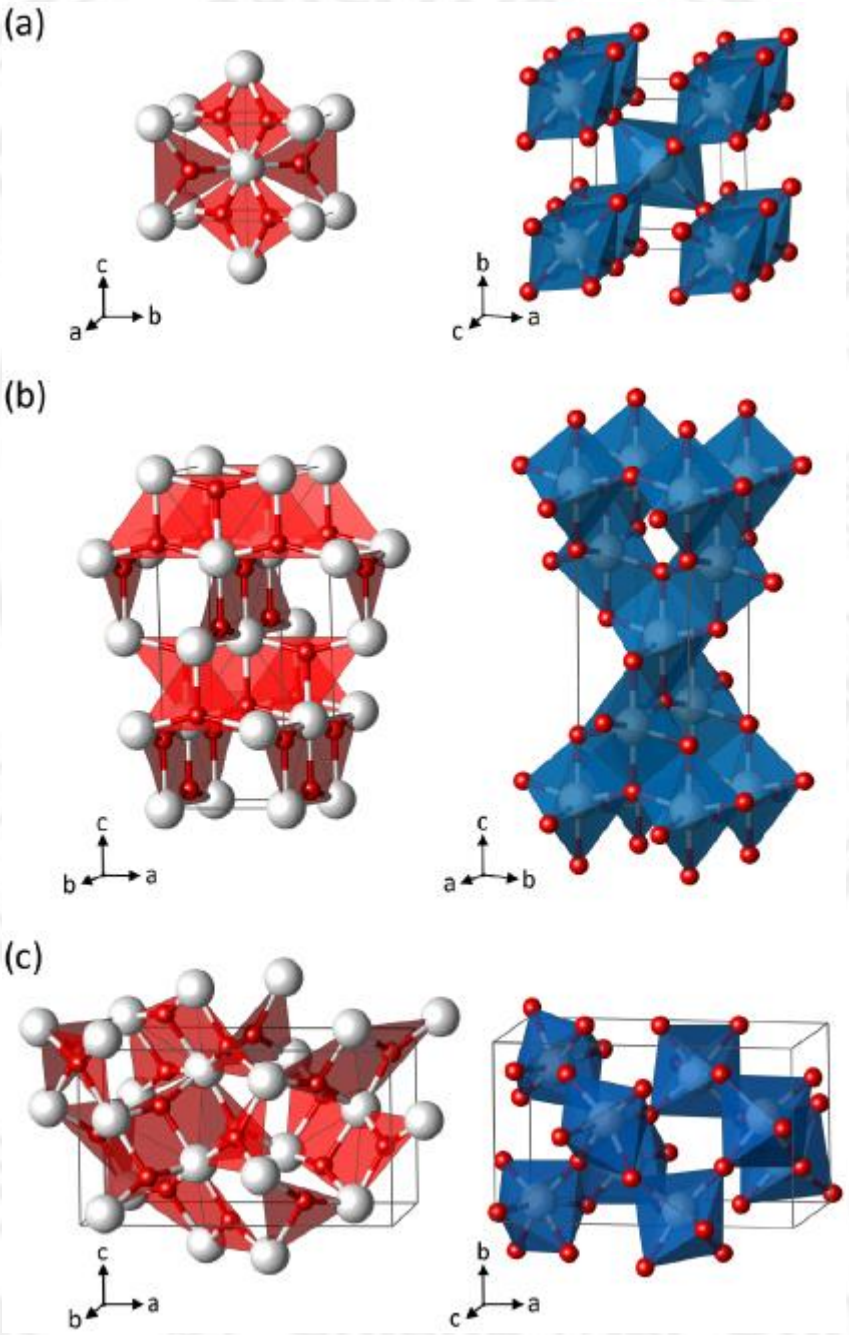

Figure 1.1 The structure of titanium dioxide in rutile phase (a), anatase phase (b) and brookite phase (c) [7]

Table 1.1 Types and physical properties of titanium dioxide [2]

Properties	**Rutile**	**Anatase**	**Brookite**
Crystalline form	Tetragonal	Tetragonal	Orthorhombic
Atomic weight	79.890	79.890	79.890
Point group	4/mmm	4/mmm	mmm
Space group	P42/mnm	I41/amd	Pbca
Density (g/cm^3)	4.27	3.90	4.13
Refractive index	2.72	2.52	2.63
Mohs'hardness	7.0-7.5	5.5-6.0	5.5-6.0
Permittivity	114	48	78
Melting point (°C)	1825	Transformation to rutile	Transformation to rutile

1.2 Electronic structure of a semiconductor

When molecular orbitals are formed from two atoms, each type of atomic orbital gives rise to two molecular orbitals. When *N* atoms are used, *N* molecular orbitals are formed. In solids, *N* is very large, resulting in a large number of orbitals. The overlap of a large number of orbitals leads to molecular orbitals that are close in energy and so form a virtually continuous band (figure 1.2). The overlap of the lowest unoccupied molecular orbitals (LUMO) results in the formation of a conduction band whereas a valence band is formed from overlapping the highest occupied molecular orbitals (HOMO). The band separation is known as the band gap (Eg), a region devoid of energy levels. From the illustration shown in figure 1.2, the reduction in the

band gap size with the formation of bands can clearly be seen. If a band is formed from the molecular overlap of *s* orbitals it is called an *s* band and likewise, an overlap of *p* orbitals, forms a *p* band and an overlap of *d* orbitals will give a *d* band. Typically, *p* orbitals have higher energy than *s* orbitals, therefore the band gap energy is formed when the two orbitals overlap. However, if the *s* and *p* bands are of similar energy, then the two bands overlap [8].

The band gap of TiO_2 anatase is 3.2 eV and rutile is 3.0 eV corresponding to an absorbance threshold of λ = 388 and 415 nm, respectively. Figure 1.3 shows the various band positions of different semiconductors. For a semiconductor to be capable of producing hydroxyl radicals, the potential of the valence band must be greater than the potential of OH•. From figure 1.3 it can be seen that ZnO, TiO_2, WO_3 and SnO_2 have the potential to produce hydroxyl radicals [4].

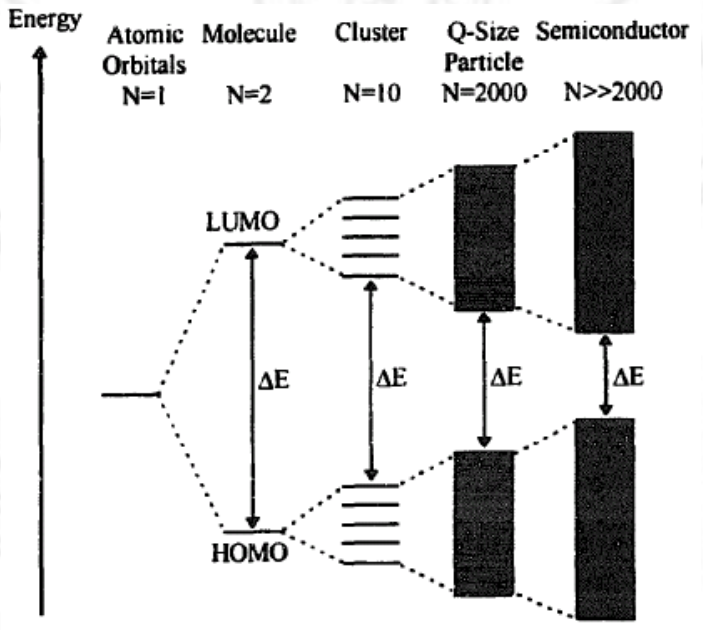

Figure 1.2 Change in the electronic structure of a semiconductor compound with increasing number of monomeric units *N* [9]

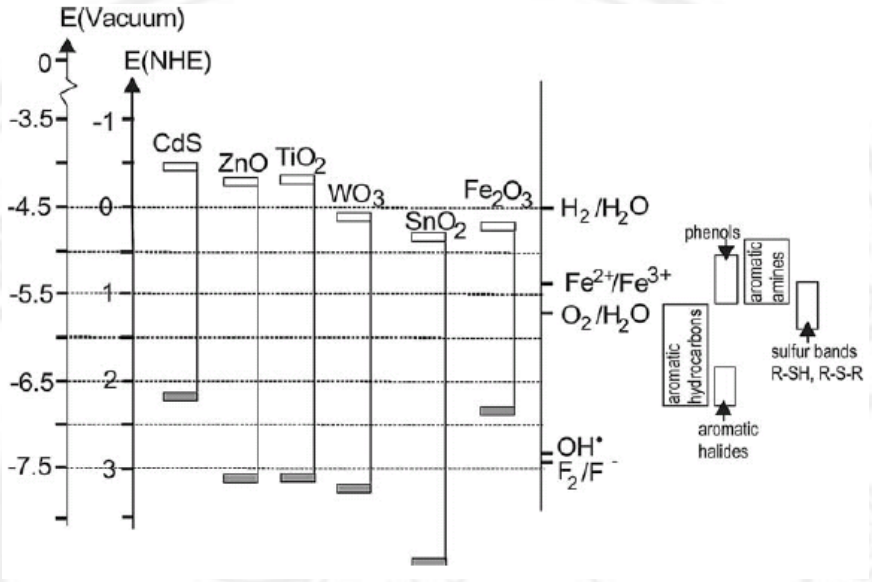

Figure 1.3 Band positions of various semiconductors and relevant redox couples [10]

Titanium dioxide is regarded as an n-type semiconductor due to the presence of oxygen vacancies in the lattice. These vacancies are formed upon the release of two electrons and molecular oxygen leaving a positive (+2) oxide ion vacancy [10]. When electrons of energy lower than the conduction band are present, the result is an n-type semiconductor (figure 1.4a). Alternatively if a material is added with atom possessing fewer electrons than the host, positive holes are added above the valence band resulting in a p-type semiconductor (figure 1.4b).

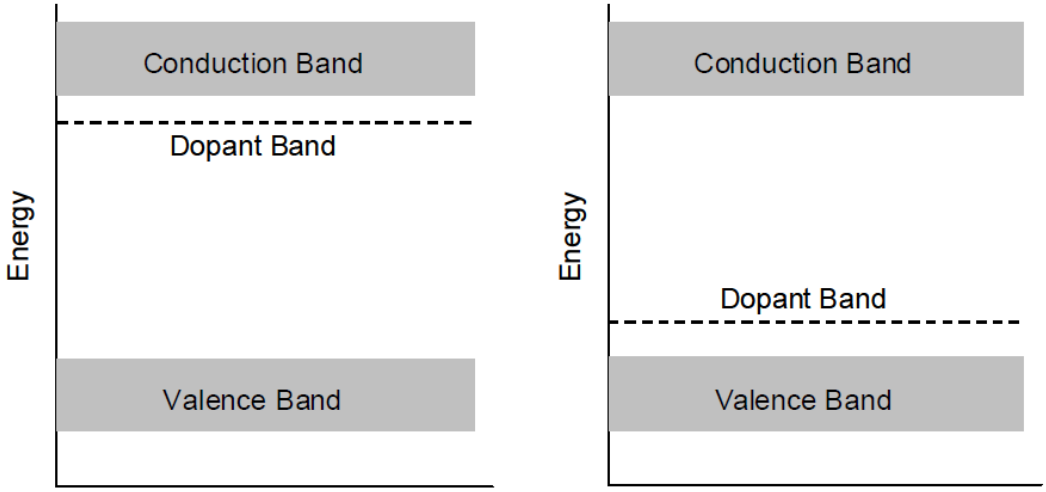

Figure 1.4 Semiconductors: n-type (a), p-type (b) [10]

1.3 Heterogeneous photocatalysis [1]

1.3.1 Semiconductors as photocatalysts

Heterogeneous photocatalysis is a process involves the occurrence of a chemical reaction in the presence of an illuminated semiconductor. A semiconductor can act as a photocatalyst due to its specific electronic structure which is characterized by a filled valence band and an empty conduction band. Figure 1.5 compares the band structure of metal, semiconductors, and insulators. The semiconductors are distinguished by the width of the energy gap. The allowable energies of electrons in a crystal are called the energy levels. In crystal with an atomic lattice, the neighboring nuclei influence the electronic structure and sharp energy levels (e.g. those associated with single atoms) become band of energy, each band representing specific quantum states. Forbidden bands exist between these bands. Electrons giving rise to chemical bonding constitute a valence band as shown in Figure 1.5.

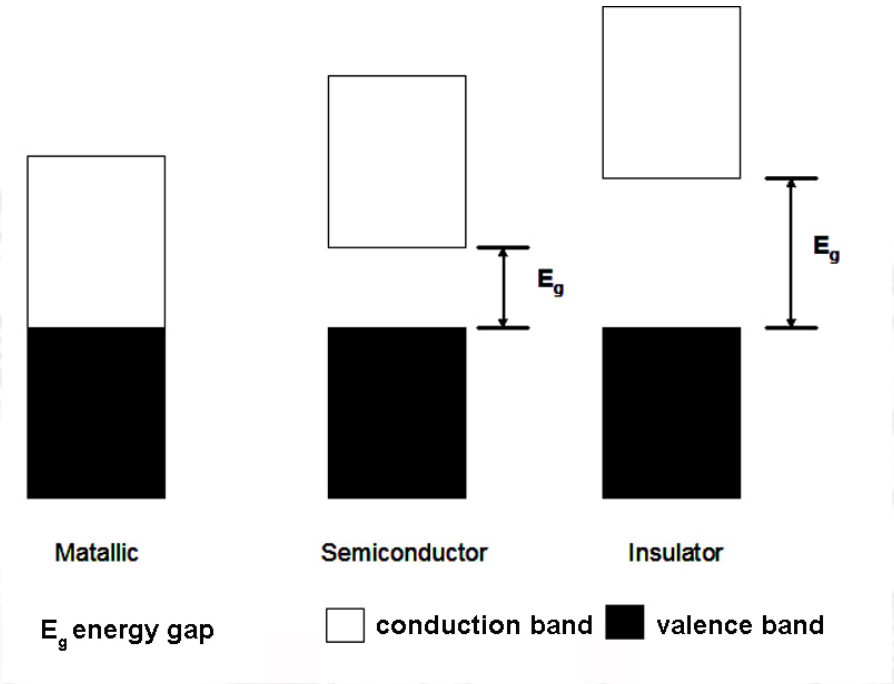

Figure 1.5 Energy band diagrams for metallic, semiconductor, and insulator [11]

The energy gap between valence band and conduction band of metallic solids are connected, therefore atoms are closely packed together. The characteristic properties of metallic conductor are high electrical and thermal conductivity, and high optical reflectivity. Whilst the insulator has a high band gap, hence the promotion of an electron from the valence band to the conduction band is difficult. The electrical conductivity of semiconductor is ordinarily much smaller than that of a metal due to the limited concentration of free electron and holes. The band gap of a semiconductor lies between a metallic solid and an insulator. Therefore, the promotion of electrons from the valence band to the conduction band, leaving holes in semiconductors, can be achieved easily relative to insulators and subsequently utilized during the photocatalytic process. In particular, TiO_2, with relatively large band gap energy of 3.0 to 3.2 eV as shown in Figure 1.6, can achieve a powerful oxidation-reduction

reaction with the ultraviolet rays present in our living environment. It is known that active oxygen and radical species existing in the presence of oxygen and water take part in the oxidation-reduction reaction.

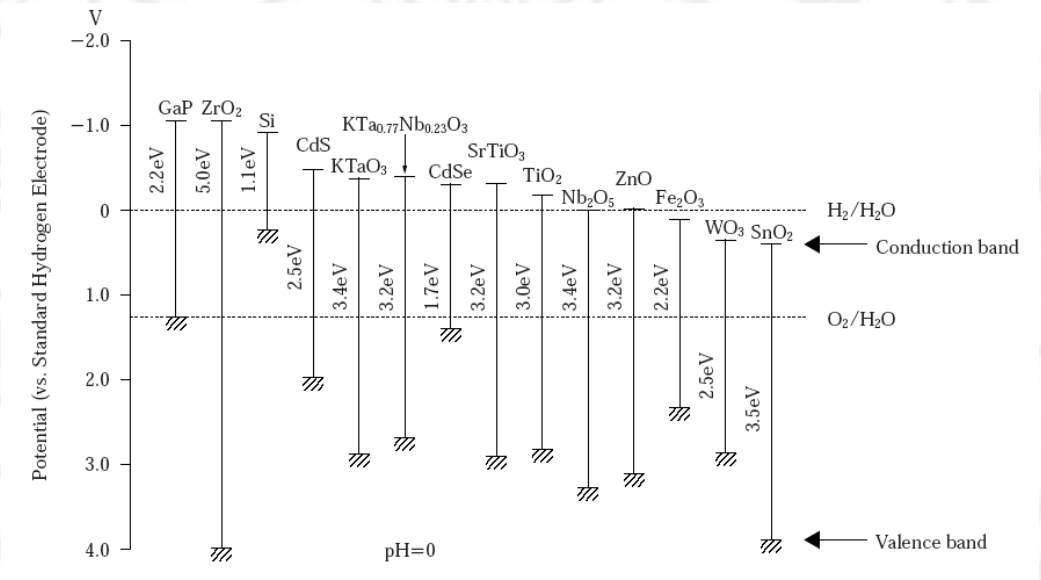

Figure 1.6 Energy structures of various photosemiconductors [12]

1.3.2 Principles of heterogeneous photocatalytic processes [1]

When a solid A, absorbs a photon of light, hν, the result is a molecule in its excited state, A$^{\cdot}$. This can be written as follows.

$$A + h\nu \quad \rightarrow \quad A^{\cdot} \qquad (1.1)$$

It is this extra energy in the molecule that allows the photocatalytic reaction to occur. Figure 1.7 shows a simplified diagram depicting the photoactivation of a semiconductor catalyst. When a semiconductor metal oxide is exposed to light, the photon energy, hν, equal to or more than the band gap (E_g) of the semiconductor is absorbed at its surface. This absorption excites the electron (e^-) resulting in their

promotion from the ground state, that is, conduction band, leaving a positive hole (h^+). The holes and electrons produced during the photoexcitation of a semiconductor are referred to as electron-hole pairs and are highly energetic and highly reactive. Figure 1.7 shows the activation of a semiconductor. The excitation with light greater than band gap energy has created an electron-hole pair and the following reactions can occur:

1. Reduction of an electron acceptor at the surface by a photogenerated electron,

2. Oxidation of an electron donor at the surface by a photogenerated holes,

3. Electron-hole recombination in the bulk or at the surface, which generated heat.

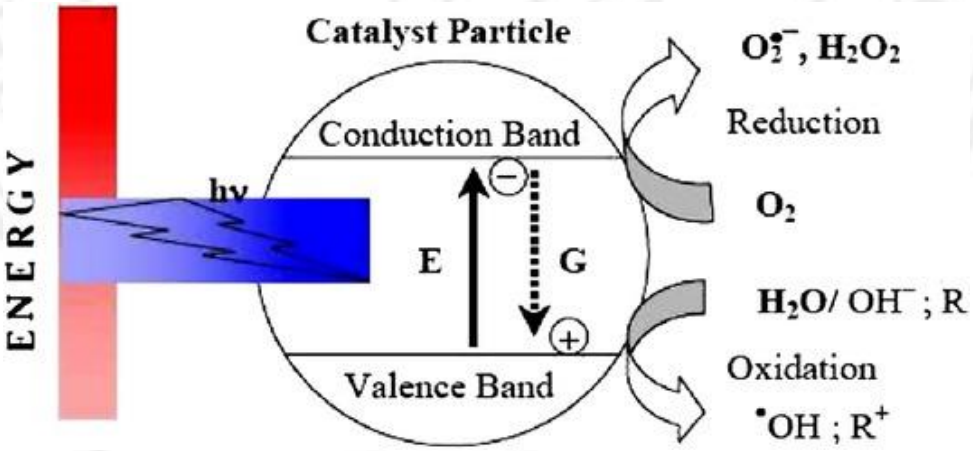

Figure 1.7 Simplified diagram of the mechanism for activation of semiconductor photocatalyst [13]

the overall process of heterogeneous catalysis can be decomposed into five independent steps: [14]

1. Transfer of the reactants in the fluid phase to the surface

2. Adsorption of a least one of the reactants

3. Reaction in the adsorbed phase

4. Desorption of the products

5. Removal of the products from the interface region

The photocatalytic reaction occurs in the adsorbed phase (Step 3). The only difference between photocatalytic reaction and conventional catalysis is the mode of activation of the catalyst in which the thermal activation is replaced by a photonic activation. The activation mode is not concerned with step 1, 2, 4 and 5, although photoadsorption and photodesorption of reactants, mainly oxygen, do exist.

Conduction band electrons (e^-) and valence band holes (h^+) are generated when photocatalyst (TiO_2) particles is irradiated with light energy equal to or greater than the band gap energy. Conduction band electrons and valence band holes migrate to the surface of catalyst where they take part in a series of redox reactions, described by the reactions below (1.2) to (1.13). Reaction (1.2) represents the formation of the charge carriers upon the illumination of the charge carriers. If these generated charge carriers are not involved in any further reactions, they can quickly recombine. The photogenerated hole can oxidize either the organic molecule directly, or the OH^- ions and H_2O molecules adsorbed at the TiO_2 surface, producing hydroxyl radicals (reaction 1.3 to 1.5). The hydroxyl radicals are the main oxidants for direct degradation of the organic compounds (D: electron donors) (reaction 1.6). The way of the oxidative leads to many case of mineralization of organic substrate to CO_2 and H_2O. The photogenerated electrons react with the dissolved oxygen to form superoxide ions (reaction 1.7). These can also form hydroxyl ions after further reactions (reactions 1.8 to 1.12). The direct reaction between the organic molecules

and the holes can also lead to the destruction of the organics (reaction 1.6). The electrons can also directly react with electron acceptors (A) (reaction 1.13)

1. Electron-hole pair generation

$TiO_2 \rightarrow TiO_2 (e^-_{cb}, h^+_{vb}) \rightarrow$ recombination (1.2)

2. Possible traps for holes

(a) Surface adsorbed water molecules

$TiO_2 (h^+_{vb}) + H_2O_{ads} \rightarrow TiO_2 + OH^{\cdot}_{ads} + H^+$ (1.3)

$TiO_2 (h^+_{vb}) + H_2O_{ads} \rightarrow TiO_2 + 1/2O_2 + H^+$ (1.4)

(b) Surface adsorbed hydroxyl ions

$TiO_2 (h^+_{vb}) + OH^-_{ads} \rightarrow TiO_2 + OH^{\cdot}_{ads}$ (1.5)

(c) Electron donor D species

$TiO_2 (h^+_{vb}) + D_{ads} \rightarrow TiO_2 + D^+_{ads}$ (1.6)

3. Possible traps for electrons

$TiO_2 (e^-_{cb}) + O_{2ads} + H^+ \rightarrow TiO_2 + OH^{\cdot}_2 \leftrightarrow O^{\cdot -}_2 + H^+$ (1.7)

$OH^{\cdot}_2 + TiO_2 (e^-cb) + H^+ \rightarrow TiO_2 + H_2O$ (1.8)

$2\ OH^{\cdot}_2 \rightarrow H_2O_2 + O_2$ (1.9)

$H_2O_2 + O^{\cdot -}_2 \rightarrow OH^{\cdot} + O_2 + OH^-$ (1.10)

$H_2O_2 + h\nu \rightarrow 2OH^{\cdot}$ (1.11)

$H_2O_2 + TiO_2(e^-_{cb}) \rightarrow TiO_2 + OH^{\cdot} + OH^-$ (1.12)

$TiO_2 (e^-_{vb}) + A_{ads} \rightarrow TiO_2 + A^+_{ads}$ (1.13)

4. Recombination

$TiO_2(e^-_{cb} + h^+_{vb}) \rightarrow TiO_2 + \text{energy}$ (1.14)

1.3.3 Photocatalytic oxidation

The photooxidation of organic compounds has been interested for many environmental such as waste water pollutant treatments. Many kinds of organic compounds have been reported to be degraded by photocatalytic process. The photooxidation of organic compounds proceeds via hydroxyl radical or directly by the photogenerated holes. Evidence that the hydroxyl radical is the main reactive oxidant in the photocatalytic degradation has been obtained by observing the intermediates of the photooxidation of halogenated aromatic compounds which are the same as those when these compounds were reacted with a known source of hydroxyl radicals [15].

1.3.4 Photocatalytic reduction

Photogenerated electrons at the conduction band of TiO_2 are relatively weaker reductants. However, the presence of added electron donor as organic hole scavenger is important in photocatalytic reduction process because it can be enhanced the reaction. In addition, hole scavengers, or some organic compounds could form reducing intermediates upon reacting with the hydroxyl radicals which could enhance the reduction reactions [16].

1.4 Factor influencing photocatalytic activity [1]

Several chemical and physical parameters have been shown to affect the photocatalytic process. Many factors influencing photocatalytic activity are such as extrinsic parameters and intrinsic parameters. Extrinsic parameters are external factors such as pH of the solution, the initial concentration of the organic compound, the light intensity, the catalyst dosage, and the temperature. The intrinsic parameters are

internal factor of photocatalyst such as the crystallographic phase, the inter-atomic spacing and the crystallite size of the catalytic material.

1.4.1 Extrinsic parameters

1.4.1.1 Light intensity

Generally, organic compound can be degraded by using TiO_2 under UV light illumination but under visible light it cannot degrade the organic compound. Therefore, light intensity has influenced the photocatalytic activity. It has also been shown that an excess of light promotes a faster electron-hole recombination. [17]

1.4.1.2 Temperature

In 1999 Herrmann [18] reported that the effect of temperature on the photocatalytic activity at the temperature ranging from 20 °C to 80 °C was not significant. This is because a photocatalyst is activated by the absorption of photon, and hence its true activation energy (E_t) is nil whereas its apparent activation energy (E_a) is often very low in this temperature range. At very low temperature such as < 0 °C, activities decrease and E_a becomes positive. This is attributed to the low temperature favoring adsorption, which is a spontaneous exothermic phenomenon. Hence, the intermediates and the final products formed could be strongly adsorbed, impeding the adsorption of the substrates to be degraded and hence decreasing the photocatalytic activity. At temperature greater than 80 °C, the exothermic adsorption process is suppressed and the adsorption of substrates becomes difficult. Under these conditions, the activity decreases and E_a tends to be negative [19].

1.4.1.3 Photocatalyst loading

The rate of chemical reaction initially increases with an increase in the catalyst loading, as this translates into an increase in the number of available active sites. The catalyst loading is an important factor in which the number of active sites depened on an optimum loading. It has been found that the optimal catalyst dosage is dependent on the light intensity as well. The higher the light intensity is, the higher the optimal catalyst loading [18].

1.4.1.4 Influence of pH

The pH of the solution has significant influences on the photocatalytic degradation process. The effect of pH on the reaction rate can be interpreted in terms of electrostatic interactions between charged TiO_2 particles and the contaminants. This in turn affects adsorption processes, since photocatalytic reactions are believed to be surface reactions. A variation in pH also affects the surface due to the amphoteric nature of titanium dioxide particles [20].

1.4.2 Intrinsic parameters [1]

1.4.2.1 Effect of surface area on photoactivity

High surface area is considered as an advantage in terms of a greater concentration of active sites per square meter, and hence leading to higher reactivity. However, it has often been reported that while the activity of the TiO_2 catalyst is affected by its external surface, photocatalytic activity is not a function of the surface area alone [21].

1.4.2.2 Effect of particle size on photoactivity

The effect of particle size on the photocatalytic activity can be interpreted in terms of its effect on the surface area which can be explained in terms of an increase in the number of active sites per square meter, as well a greater adsorption ability of the pollutants on the catalyst surface [22].

1.4.2.3 The importance of the crystal structure

Anatase phase is normally employed to degrade the organic compounds which due to its higher active sites than rutile and brookite phases. Some researchers reports have proposed that the high degree of hydroxylation is one of the most important characteristic for anatase phase when compared with rutile phase [23].

1.5 Improvement of photoactivity

In order to improve efficiency of photocatalysis, several techniques of material modification have been explored. As physical properties of materials influence the photoactivity, different physical properties of surface or structure such as nanoparticle, nanotube, defect disorder, including layered and core-shell structure would be useful [23].

1.5.1 Decreasing the band gap (visible light activated TiO_2) [24]

A major drawback of TiO_2 photocatalysis is the large band gap. Titanium dioxide can only be activated upon irradiation with a photon of light <390 nm, limiting its use under UV irradiation [25]. Ultraviolet light makes up 3 - 5 % of the solar spectrum, whereas the spectrum consists of ~ 40 % visible light. Therefore, in

order to utilise TiO_2 to its full potential it is necessary to decrease the band gap size facilitating visible light absorption. Non-metal doping has shown great promise in achieving visible light-activated photocatalysis, with nitrogen being the most effective dopant. Kuo *et al* [25] were the first to show visible light absorption through N doping. They reported that nitrogen-doped TiO_2 promoted photocatalytic activity up to $\lambda = 520$ nm [26]. The nitrogen substitutional doping of TiO_2 was early claimed as a method for narrowing the band gap by exclusively changing the valence band structure; fine electronic details of this are however under discussion. Kuo [25] et al claimed that the presence of nitrogen narrows the band gap of TiO_2 thus making it capable of performing visible light driven photocatalysis[26]. However, Ihara et al suggested that it is the oxygen vacancies that contributed to the visible light activity, and the doped nitrogen only enhanced the stabilisation of these oxygen vacancies[27]. They also confirmed this role of oxygen vacancies in plasma-treated TiO_2 photocatalysts. In addition the structural oxygen vacancy caused visible light photocatalytic activity was also reported by Martyanov *et al* [28]. Currently there appears to be some agreement on the mechanism of nitrogen doped visible light absorption explained by Irie [26]. They explained that TiO_2 oxygen lattice sites substituted by nitrogen atoms form an occupied midgap (N-2p) level above the (O-2p) valence band (figure 1.8). Irradiation with UV light excites electrons in both the valence band and the narrow (N-2p) band, but irradiating with visible light only excites electrons in the narrow (N-2p) band [26]. It has also been shown that F doping improves both UV and visible light photocatalytic activity. However, their mechanisms are still under discussion.

Previous studies have shown that N-F-codoped TiO_2 powders demonstrated excellent photocatalytic activity no matter what kind of light source was used. This seems to be a consequence of the perfect combination of some beneficial effects induced by both N and F dopants. Carbon, phosphorous and sulfur have also shown positive results for visible light responsive TiO_2 [29]. The non-metal dopants effectively narrow the band gap of TiO_2 (< 3.2 eV) [30]. Change of the lattice parameters and the presence of trap states within the conduction and valence bands from electronic perturbations give rise to band gap narrowing [31]. Not only does this allow for visible light absorption but the presence of trap sites within the TiO_2 bands increases the lifetime of photoinduced charge carriers.

Doping of TiO_2 with transition metals such as Cr, Co, V and Fe have extended the spectral response of TiO_2 well into the visible region and also improve photocatalytic acitivity [32]. However, transition metals may also act as recombination sites for the photo induced charge carriers thus, lowering the quantum efficiency. Transition metals have also been found to cause thermal instability to the TiO_2 nanomaterials [33]. Kang argues that despite the fact that a decrease in band gap energy has been achieved by many groups through metal doping, photocatalytic activity has not been remarkably enhanced because the metals introduced were not incorporated into the TiO_2 framework. In addition, metals remaining on the TiO_2 surface cover photo reaction sites [34].

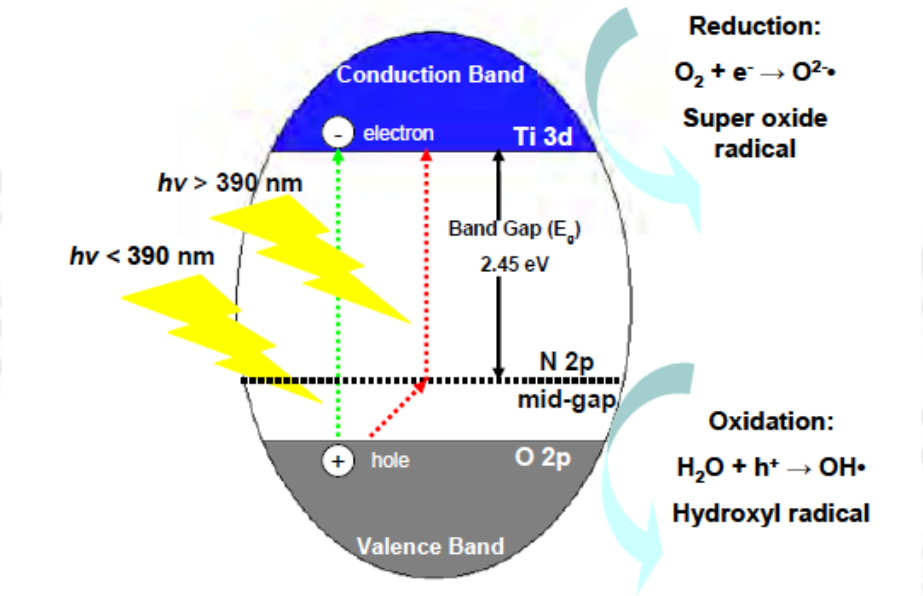

Figure 1.8 Schematic diagram of N-doped TiO_2 photocatalysis [26]

1.5.2 Chemical modification [24]

The reaction rates of hydrolysis and condensation reactions associated with sol-gel synthesis can easily be altered. Chemical modification of titanium alkoxides will retard hydrolysis and condensation reactions, allowing for greater control over the reaction and evolving polymeric species [35]. Modification typically occurs through a nucleophilic substitution (S_N) reaction. A new molecular precursor is produced upon the reaction of a nucleophilic reagent (XOH) with a metal alkoxide.

$$XOH + M(OR)_z \rightarrow M(OR)_{z-x}(OX)_x + xROH \quad (1.15)$$

If M is coordinatively unsaturated (N – z >1) by nucleophilic addition (AN), then:

$$XOH + M(OR)_z \rightarrow M(OR)_z(XOH)_{N-z} \quad (1.16)$$

When δ(M) >>1, (N – z) > 1, and (XOH) is a strong nucleophile, the reactivity of the alkoxide towards this modification is increased [36]. The hydrolysis and condensation behaviour of the modified precursor depends on the stability of the modifying ligands.

In a typical modified synthesis, alkoxide ligands that are less electronegative are preferentially removed during hydrolysis. The modifying ligands which tend to be more electronegative will remain throughout the hydrolysis and are only removed during condensation [37]. In modified precursors, stable modifying ligands cause the effective functionality toward condensation to be reduced, altering the condensation pathway and resulting in less highly condensed products and promoting gelation [37].

Alcohol exchange reactions can readily occur with metal alkoxide precursors:

$$M(OR)z + xR'OH \rightarrow M(OR)z\text{-}x(OR')x + xROH \quad (1.17)$$

therefore, alcohol exchange is known to be a common method of alkoxide synthesis. When $\delta(M) >> 1$ and when R' is less sterically bulky than R, alcohol exchange will proceed. Alcohol exchange rates decrease as alkoxy chain length increases, MeOH > EtOH > Pr^iOH > Bu^tOH. [35] As hydrolysis rates decrease with steric bulk of the alkoxy ligands, chemical modification of transition metal precursors may involve exchanging a bulky ligand for a less bulky one. The hydrolysis behaviour of transition metal alkoxides can be significantly altered through alcohol exchange. Precipitation occurs when relatively small alkoxy ligands such as $Ti(OE^t)_4$ or $Ti(OPr^i)_4$ are hydrolysed with excess water (r > 2). Whereas stable sols are obtained with the bulky $Ti(OAm^t)_4$, (OAm^t = amyl alcohol, $C_5H_{11}OH$). In the mixed alkoxide, $Ti(OPr^i)_{4-x}(OAm^t)_x$, the (OAm^t) group is less electronegative than (OPr^i). As hydrolysis preferentially occurs on less electronegative ligands, (OAmt) is preferentially hydrolysed and rapid gelation occurs [38].

Acetic acid (HOAc) is commonly used to modify titanium alkoxides. Reacting of HOAc with metal alkoxides leads to the formation of metal alkoxo-acetates [39], [40]. The addition of HOAc increases the gel time for $Ti(OR)_4$ as explained below

[38]. Livage and coworkers [35] have performed many experiments on acetic acid modified $Ti(OR)_4$. They have combined X-ray absorption near edge spectroscopy (XANES), ^{13}C NMR, IR and X-ray absorption fine structure (EXAFS) and have made several breakthroughs regarding the structure and behaviour of HOAc modified titanium alkoxides. They have shown that $Ti(OPr^i)_4$ consists of monomeric units and the Ti atom exhibits a coordination number, N = 4. Upon addition of glacial acetic acid an exothermic reaction occurs. XANES experiments indicated that the coordination number of the central titanium atom, N, instantaneously increases to 6. ^{13}C NMR showed that the chemical environments of the carboxylic and methyl carbons in the HOAc were altered after the reaction with $Ti(OPr^i)_4$. It is believed that this is due to the HOAc bonding with the titanium and not the OPr^i groups. However, both bridged and terminal OPr^i ligands remain are present (figure 1.9). The IR spectrum of the reaction product exhibits absorption bands due to titanium alkoxide, acetic acid and the propyl acetate ester. Also, there are two strong bands at ~ 1500 cm^{-1} assigned to the symmetric and antisymmetric stretching vibrations of ridging carboxylic groups: $\nu_s(CO_2^-)$ = 1450 cm^{-1} and $\nu_a(CO_2^-)$ = 1580 cm^{-1}. The frequency difference ($\Delta\nu$ = 130 cm^{-1}) is typical of an acetate ion acting as a bidentate ligand. IR also confirms the presence of both terminal (1084 cm^{-1}) and bridging (1034 cm^{-1}) OPr^i ligands. This evidence combined with a Ti-Ti correlation of 3.05 Å determined from EXAFS is consistent with a dimer composed of bridging and terminal OPr^i ligands and bridging CH_3COO^- ligands as shown in figure 1.9. During hydrolysis, ^1H and ^{13}C NMR and IR spectroscopy indicated that OPr^i groups are preferentially hydrolysed [35], whereas the bridging acetate ligands remain bonded to titanium throughout much of the condensation process. Since the bridging CH_3COO ligands are not

hydrolysed, they effectively alter the condensation pathway perhaps promoting the formation of linear polymers composed of edge shared octahedral [37]. The formation of the edge shared octahedra stabilise TiO_2 as anatase [35].

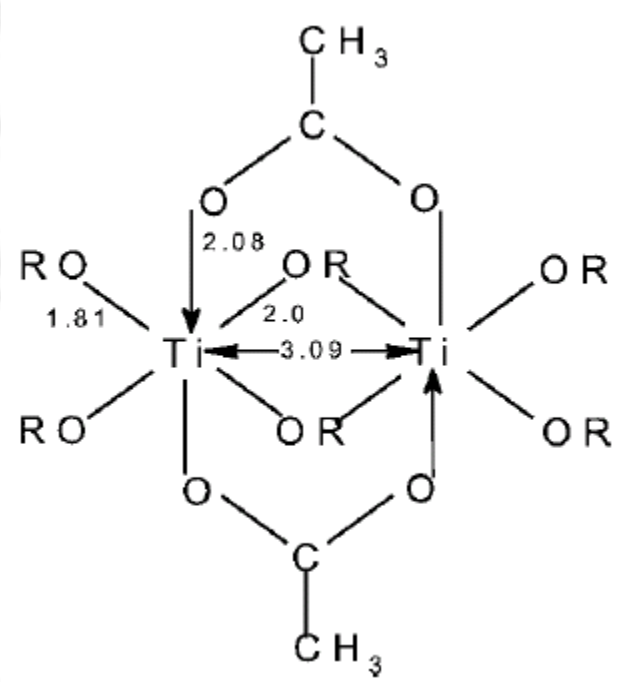

Figure 1.9 Proposed structure of titanium acetate [35]

An alternative chemical modifier, formic acid is also employed as a chelating agent for the synthesis of titanium dioxide using titanium isopropoxide. Formic acid was chosen because it is the simplest carboxylate species and because of its similar structural properties to acetic acid. Initially it was assumed that titanium dioxide may be synthesised with formic acid in a similar manner to that of acetic acid and as such it was decided that the same synthesis route will be employed but with varying ratios of precursor:formic acid:water. The carboxylate coordinations include: ionic, monodentate, bidentate chelating and bridging [41]. From FTIR and Raman spectroscopy, the role of the chelating agent in the synthesis was examined. Ivanda et

[42] al carried out spectroscopic studies on powders synthesised from an esterfication reaction to find bridging of various carboxylates. However, the paper focused mainly on particle size as opposed to relating oligomeric structure and anatase to rutile transformation temperatures [42]. FTIR and Raman spectroscopy can be used to determine the mode of the carboxylate binding (figure 3.10). The frequency of the asymmetric carboxylate vibration in the IR spectra, $\nu_{as}(COO^-)$, and the magnitude of the separation between the carboxylate stretches, $\Delta = \nu_{as}(COO^-) - \nu_s(COO^-)$, are often used as spectroscopic criteria to determine the mode of the carboxylate binding [41].

Generally the following order is proposed for divalent metal carboxylates: Δ (chelating) < Δ (bridging) < Δ (ionic) < Δ (monodentate) [41] Δ ionic is reported as 160 - 170 cm^{-1} for acetates and 200 - 210 cm^{-1} for formats [43]. In the monodentate coordination, electron density redistribution occurs and the shift of $\nu_{as}(COO^-)$ to higher wavenumbers is observed in comparison with the ionic group, increasing the value of Δ. The chelating coordination, however, shifts the position of the asymmetric carboxylate stretch to lower wavenumbers in comparison with the ionic group and thus lowers the value of Δ. In the bridging coordination, one divalent metal cation is bound to one of the oxygen atoms of the COO^- group and another divalent metal cation to the other oxygen, the asymmetric stretch is located at the same position as that of the ionic group [41], [44]. The range 200 - 210 cm^{-1} was derived for ionic formates and in general the comparison of the Δ value of the respective complex with the Δ value of the sodium salt should be used for the assignment following the guidelines: (i) bidentate chelating coordination: $\Delta(COO^-)_{studied\ complex} << \Delta(COO^-)_{sodium\ salt}$; (ii) bidentate bridging carboxylate: $\Delta(COO^-)_{studied\ complex} \leq \Delta(COO^-)_{sodium\ salt}$; (iii) monodentate coordination: $\Delta(COO^-)_{studied\ complex} >> \Delta(COO^-)_{sodium\ salt}$ [40], [43].

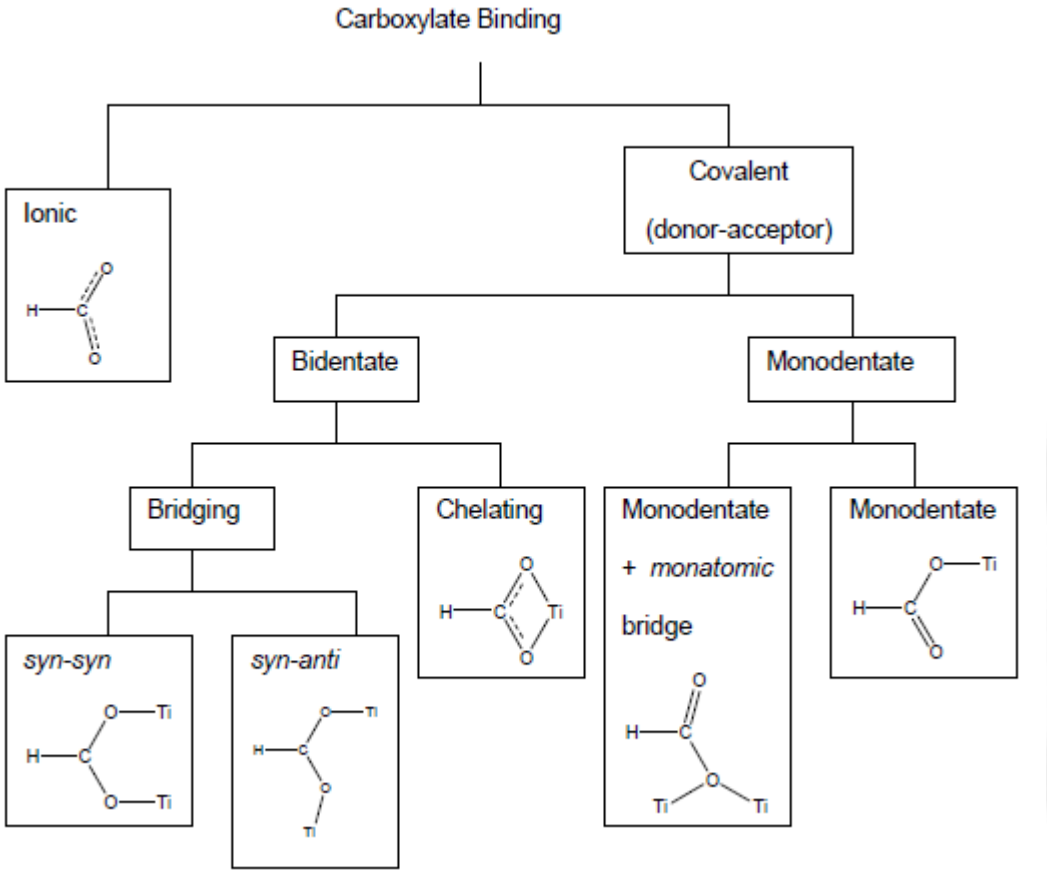

Figure 1.10 Modes of carboxylate binding [41]

1.6 Synthesis techniques [1]

1.6.1 Hydrothermal synthesis

Hydrothermal synthesis is typically carried out in a pressurised vessel called an autoclave with the reaction in aqueous solution [45]. The temperature in the autoclave can be raised above the boiling point of water, reaching the pressure of vapour saturation. Hydrothermal synthesis is widely used for the preparation of TiO_2 nanoparticles which can easily be obtained through hydrothermal treatment of peptised precipitates of a titanium precursor with water [45]. The hydrothermal method can be useful to control grain size, particle morphology, crystalline phase and

surface chemistry through regulation of the solution composition, reaction temperature, pressure, solvent properties, additives and aging time [10].

1.6.2 Solvothermal method

This method employs chemical reactions in organic media such as methanol, 1,4 butanol, toluene under self-produced pressures at relatively low temperatures (usually under 250 °C). The solvothermal method could be beneficial to control particle size, particle morphology, and crystalline phase. Moreover, the surface chemistry properties can be controlled by using the solution composition, reaction temperature, pressure, solvent properties, additives, and ageing time as in the case of hydrothermal method [47], [46].

1.6.3 Impregnation method

Impregnation method is the simple method of making a catalyst. The powder of catalyst is contacted with an aqueous or organic solution then dried and calcined. The impregnation technique requires less equipment since the filtering and forming steps are eliminated and washing may not be needed. It is the preferred method in preparing metal ions coating on surface of semiconductors such as TiO_2, ZnO, and SnO_2 due to its simplicity [48].

1.6.4 Microwave synthesis

Various TiO_2 materials have been synthesised using microwave radiation. Microwave techniques eliminate the use of high temperature calcination for extended periods of time and allow fast, reproducible synthesis of crystalline TiO_2

nanomaterials. High quality rutile rods were developed combining hydrothermal and microwave synthesis, while TiO_2 hollow, open ended nanotubes were synthesised through reacting anatase and rutile crystals in NaOH solution [46b].

1.6.5 Sol-Gel processing

Sol-gel processing is a common chemical approach to produce high purity materials shaped as powders, thin film coatings, fibers, monoliths and self-supported bulk structures [49]. The sol-gel method has several advantages over other synthesis techniques such as purity, homogeneity, stoichiometric control, ease of preparation and ease of introducing dopants, composition and the ability to produce thin film coatings or porous powders. There are two possible routes for carrying out sol-gel synthesis, the non-alkoxide route and the alkoxide route. The non-alkoxide route uses inorganic salts ($TiCl_4$) as the starting material. This requires the removal of the inorganic anion to produce the required oxide (titanium dioxide). However, halides often remain in the final oxide material and are difficult to remove. The alkoxide route involves hydrolysis of a metal alkoxide, followed by condensation. The hydrolysis/condensation reactions typically form a three dimensional polymeric structure, that, upon calcination will result in anatase or rutile titanium dioxide crystals depending on the calcination temperature. The alkoxide route is used throughout this thesis and it will be explained in greater detail in the following section.

1.7. Applications of TiO_2 [1]

1.7.1 Photocatalytic splitting of water

Since Fujishima and Honda carried out the photocatalytic splitting of water using TiO_2 in 1972 [50], great effort has gone into maximising the potential of the process as it can provide clean renewable energy from sustainable sources [45]. Figure 1.11 shows a schematic presentation of the principle of water splitting using a TiO_2 photocatalyst. Light of energy greater than the band gap excites an electron from the valence band to the conduction band. The photogenerated electron/hole pair causes redox reactions. Water molecules are reduced by excited electrons to form H_2 and oxidised by holes to form O_2 leading to water splitting [51].

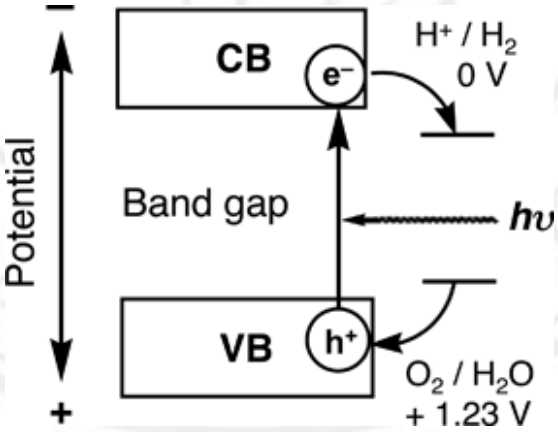

Figure 1.11 TiO_2 photocatalytic splitting of water [51]

1.7.2 The dye sensitised solar cell

The dye sensitised solar cell (DSSC) has shown great potential as the next generation of solar cells. The DSSC has several advantages over current photovoltaic cells such as; low production costs, more consistent energy production from diffuse

and direct sunlight, colour choice and transparency (figure 1.12). Also, because the DSSC utilises TiO_2 nanoparticles, solar cells of much smaller sizes can be produced and they can even be flexible [52].

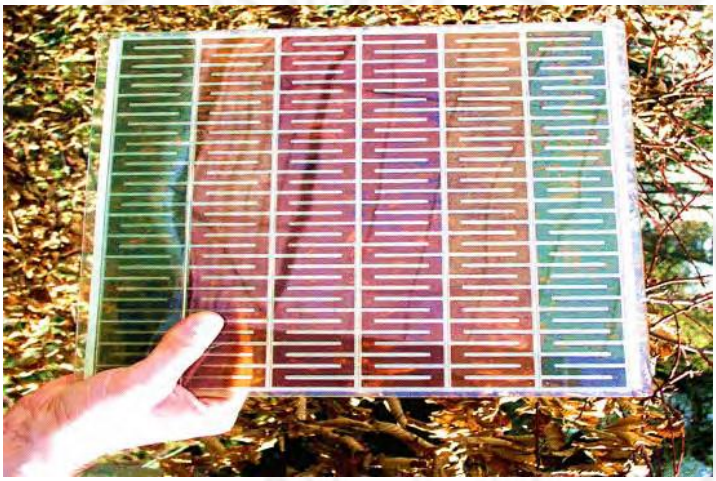

Figure 1.12 Pictures of the dye sensitised solar cell [53]

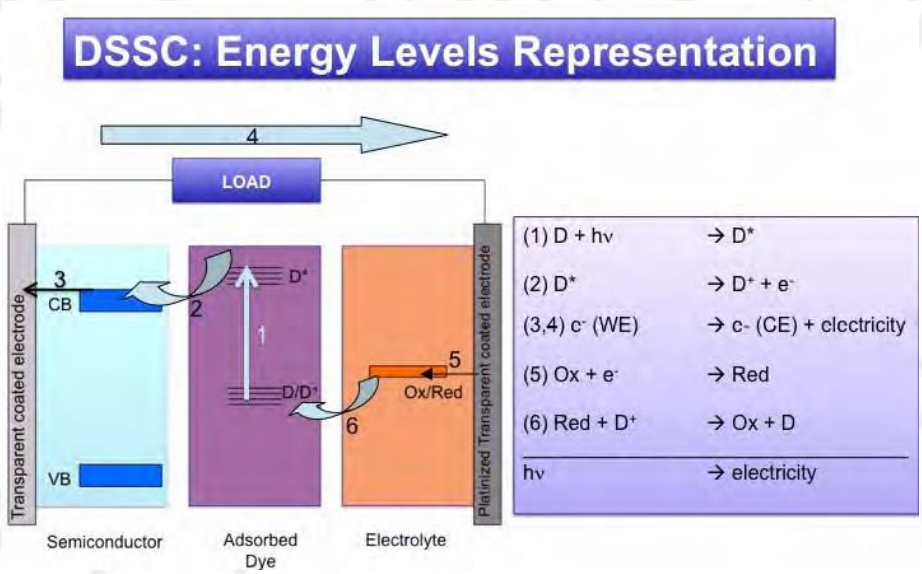

Figure 1.13 Schematic diagram of a DSSC showing energy levels and electronic transitions [54]

The DSSC mimics nature's photosynthetic process of light absorption and electron injection. In the DSSC (figure 1.13), light is absorbed by a coloured dye (commonly ruthenium based dye), to produce an excited singlet state. Excited electrons from the dye are then injected into the conduction band of the TiO_2 support. Following successful injection, the electron percolates through the oxide layer onto the working electrode. Once the electron reaches the electrode it will travel to the counter electrode, therefore generating an electrical current. The electrolyte contains a redox couple (1,2-dimethyl-3-propylimidazolium iodide, iodine, N methylbenzimidazole, I^-/I_3^-) which will regenerate the oxidised dye, allowing for the process to start again.

A significant drawback of the DSSC is the electronic processes that compete with injection from the dye to the TiO_2 working electrode. The main competitive pathway is that of electron recombination in the dye. So instead of the dye excited electron transferring to the conduction band of the TiO_2, it will relax to the ground state of the dye. Therefore, for the full potential of DSSC energy production to be realised it is necessary for researchers to produce TiO_2 with enhanced electron collection abilities [55]. As TiO_2 synthesis reactions are better understood it may become possible to design synthesis techniques that will produce TiO_2 materials capable of enhanced electron capture properties.

1.7.3 Photocatalytic degradation of pollutants

Titanium dioxide has attracted great interest in the past decade due to its environmental applications such as air purification and water remediation. The photocatalytic mechanism is activated by light with the energy greater than that of the

semiconductor band gap. Upon photo-activation, an electron-hole pair is produced that reacts with adsorbed species to produce radical species. These radicals are powerful oxidising agents which will oxidise organic contaminants to CO_2 and H_2O [55].

1.8 Literature review

In 1997, Sato *et al*. [56] studied pore size regulation of TiO_2 obtained from *in-situ* modification. Titanium precursor, solvent and organic modifier used in their work are titanium tetraisopropoxide ($Ti(OPr)_4$), propan-1-ol and stearic acid, respectively. The molar ratios of $Ti(OPr)_4$, stearic acid, and propan-1-ol were 1: *X*: 26, where *X* was varied from 0 to 2. The precipitate was then calcined at 400, 500 and 600 ^oC for 24 h. Crystal structure of the sample calcined at 500°C, as confirmed by XRD, was anatase TiO_2. The pore diameter was increased from 5 to 15 nm upon increasing the stearic acid/Ti molar ratio from 0.3 to 1.2. The results clearly suggested that pore size distribution of TiO_2 can be controlled by varying stearic acid/Ti molar ratio. High amount of stearic acid led to the increase of specific area and pore size, thus resulting enhanced adsorption ability of TiO_2 towards organic pollutant.

In 2000, Takenaka *et al.* [57] prepared mesoporous titania from titanium alkoxide and monofunctional carboxylic acids, with different alkyl chain length ($CH_3(CH)_nCOOH$, where *n* was varied from 0 to 20). The molar ratio of titanium alkoxide, carboxylic acid and propan-1-ol was 1: 1.5: 26. Results from XRD analysis indicated the presence of anatase TiO_2 when the sample was calcined at 400 ^oC for 4h. The functional group and type of bonding were examined by Fourier transform infrared spectroscopy (FTIR). Two absorption peaks around 1400-1500 cm^{-1} and

1500-1600 cm^{-1} assigned to symmetric and asymmetric stretching vibration of a bidentate carboxylate ligand (COO^-) were found from the carboxylic acid-modified sample. The specific surface area, pore volume and pore size were increased with increasing *n* of monofunctional carboxylic acids.

In 2003, Bessekhouad and *et al.* [58] prepared TiO_2 by emulsification-gelation technology, hydrolysis and reflux process. The starting precursor (Tetraisopropylorthotitanate $Ti(OC_3H_7)_4$) was modified by 1,4 cyclohexane diol ($C_6H_{14}O_2$), hydrogen peroxide (H_2O_2) and Triethanol amine ($C_6H_{15}NO_3$). Titanium tetrachloride was also used as a precursor. The obtained products were treated at 550 ˚C for 2 or 10 hours in air, the product calcined for 10 h at 550 ºC showed a single anatase phase with 10 nm crystallite size. TiO_2 nanoparticles with a crystallite size between 8 nm and 40 nm were successfully prepared. The photoactivity of TiO_2 was investigated using benzamide as the representative aromatic pollutant. It was founf that the best photoactivity was obtained from the product prepared by reflux process and heated at 550 ºC for 10 h. In the same year, Kolen'ko *et al.*[59] prepared nanocrystalline TiO_2 powders from aqueous $TiOSO_4$ solutions under hydrothermal conditions. Results from XRD analysis indicated the presence of anatase phase after hydrothermal treatment at 423 for 6h. The increase of the reaction time and temperature resulted in a considerable increase of crystal size from 8 to 28 nm. High temperature hydrolysis of $TiOSO_4$ solution result in high crystallinity, high specific surface area were increase photocatalytic degradation of pollutant.

In 2004, Su *et al.* [*60*] studied the sol–gel preparation and photocatalysis of titanium dioxide. Titanium dioxide was prepared by the hydrolysis and condensation of titanium (IV) n-butoxide in iso-propyl alcohol. The XRD peaks showed rutile

phase became the major constituent of TiO_2 when increasing calcination temperature to 700 °C. The XRD data showed the crystal size of TiO2 in the range of 4-35 nm and BET surface area recorded a significant decrease from 122 to 11.5 m^2g^{-1}.

In 2006, Yang *et al.* [61] studied the sol-gel preparation and photocatalysis of titanium dioxide. The starting materials were AR-grade $Ti(OBu_4)$ and anhydrous alcohol. The powder was then further calcined at 500 and 650 ^oC for 2h. Results from XRD analysis indicated the presence of anatase phase after calcined at 500 ^oC and mixed phase of rutile and anatase was found after calcined at 650 ^oC for 2h. The nanoparticles have a spherical morphology with an average diameter of ca. 20 nm. The photocatalytic degradation of methyl orange over TiO_2 calcined at 650^oC showed significantly higher efficiency than that of the commercial TiO_2 calcined at 500 ^oC. In the same year, Wahi *et al.* [62] prepared ultrahigh surface of anatase TiO_2 by solvothermal method. Ultrafine nanocrystalline anatase with high specific surface area (up to 250 $m^2\ g^{-1}$) was obtained upon injection of a titanium alkoxide precursor into ethanol with designed volume of water under mild solvothermal conditions. Results from XRD analysis indicated the presence of anatase phase after hydrothermal treatment at 140-400 ^oC for 2h. The specific surface area was decrease with increasing the thermal treatment. Sakthivel *et al* [63] prepared TiO_2 by simple hydrolysis method from titanyl sulphate ($TiOSO_4$). Parameters affecting the physical and chemical properties of TiO_2 are such as pH, calcination temperature, hydrolysing agent and ageing time. The optimum condition was at pH 5.5 with the use of sodium hydroxide as a hydrolysing agent and an ageing time of 24 h. The photocatalytic degradation of dichloroacetic acid over TiO_2 calcined at 400^oC showed significantly higher efficiency than that of the commercial TiO_2 Degussa P25.

In 2008, Tian *et al.* [64] prepared mesoporous TiO_2 from industrial $TiOSO_4$ solution via hydrothermal method, using cetyltrimethylammonium bromide (CTAB) and tri-block copolymer $EO_{20}PO_{70}EO_{20}$ (P-123) as structure-directing agents (SDA) under high acidic conditions. The molar ratio of Ti/CTAB/P-123 was 1: 0.1: 0.01. The rates of hydrolysis and condensation of industrial $TiOSO_4$ were controlled by adjusting the pH value of the reacting system. The mixed solution was subjected to hydrothermal treatment in an autoclave at 393 K for 12 h. The powder was then further calcined at 623 K, 673 K, 723 K, 773 K and 823 K for 2 h to remove the structure-directing agents. As the calcination temperature increased, the peaks shifted to the lower angle, corresponding to the increasing of *d*-spacing due to pore wall compacting and template removal. The powder calcined at 723 K for 2 h showed higher thermal stability, with BET specific surface area of 218.7 m^2/g and an average pore diameter of 3.63 nm.

In 2010, Štengl *et al*. [65] prepared TiO_2 by homogeneous hydrolysis of $TiOSO_4$ aqueous solutions in the presence of CTAB and SDBS, respectively. The prepared samples were heated to 600°C for 1 h to remove residual surfactants. The XRD results of sample showed pure anatase phase and the crystallite size decreased with an increased amount of surfactants. The surface area, pore volume and pore radius increased upon increasing the amount of surfactant during the preparation. The resulting mesoporous titania showed significantly higher photocatalytic degradation of dye than that of the reference samples prepared without surfactants and of the commercial TiO_2 Degussa P25. In the same year, Sharabi and Paz. [66] studied molecular imprinting on titanium dioxide using diisopropyl methylphosphonate (DIMP) and diethylhydroxymethylphosphonate (DEHMP) for molecular imprinting

and studied the photocatalytic degradation of organic compounds. The molar ratio between TiO_2 and phosphonate are 1:5. Crystal structure of the sample, as confirmed by XRD, was anatase TiO_2. Photocatalytic activity of the imprinted sample was significantly higher than that of the non-imprinted sample possibly due to the higher specific area.

1.9 Research problem and aim

TiO_2 has been used to degrade various organic compounds such as carboxylic acids [67], organic dyes [68], herbicides and pesticides [69]. However, when using TiO_2 to degrade aromatic hydrocarbons, low photoactivity is usually obtained due to the poor adsorption ability and capacity towards non polar compound of TiO_2. Therefore, improving these properties towards aromatic compounds could help increase photocatalytic performance.

The adsorption of TiO_2 towards desired molecules can be improved either by *in-situ* or post modification approach [70]. In an *in-situ* modification, the attachment of modifier molecules onto TiO_2 nanoparticles is finished during the growth of TiO_2 nanocrystals. By using this method, TiO_2 with controllable pore size and thus desired adsorption ability can be obtained by varying the amount and type of organic modifiers added. In the post modification method, TiO_2 nanoparticles are firstly prepared, and then surface modified by organic modifiers. However this approach encounters low photostability of the organic modifier on TiO_2 surface which is an important problem in photocatalytic application. Therefore, an *in-situ* modification has usually been employed.

In this study, TiO_2 will be *in-situ* modified by chemical solution method using titanyl sulphate ($TiOSO_4$) as a titanium precursor. Organic modifiers used in this work are of aromatic carboxylic acids. The obtained sample will also be investigated for its photocatalytic activity under UV light irradiation.

1.10 Research Objectives

1. To synthesize TiO_2 by thermal hydrolysis of $TiOSO_4$

2. To *in-situ* modify TiO_2 with some selected carboxylic acids

3. To investigate physical and chemical properties of the obtained materials

4. To study the photocatalytic degradation of phenol over the prepared catalysts

REFERENCES

1. Wetchakun, N., Effect of transition metal ion doping on the photocatalytic activity of titanium dioxide. *The Graduate School Chiang Mai University* **2008**, 1-72.
2. Gai, P. L.; Boyes, E. D.; Helveg, S.; Hansen, P. L.; Giorgio, S.; Henry, C. R., Atomic-resolution environmental transmission electron microscopy for probing gas–solid reactions in heterogeneous catalysis. *MRS bulletin* **2007,** *32* (12), 1044-1050.
3. Wisitsoraat, A.; Tuantranont, A.; Comini, E.; Sberveglieri, G.; Wlodarski, W., Characterization of n-type and p-type semiconductor gas sensors based on NiO_x doped TiO_2 thin films. *Thin Solid Films* **2009,** *517* (8), 2775-2780.
4. Asahi, R.; Taga, Y.; Mannstadt, W.; Freeman, A., Electronic and optical properties of anatase TiO_2. *Physical Review B* **2000,** *61* (11), 7459.
5. Amtout, A.; Leonelli, R., Optical properties of rutile near its fundamental band gap. *Physical Review B* **1995,** *51* (11), 6842.
6. Li, J.-G.; Ishigaki, T.; Sun, X., Anatase, brookite, and rutile nanocrystals via redox reactions under mild hydrothermal conditions: phase-selective synthesis and physicochemical properties. *The Journal of Physical Chemistry C* **2007,** *111* (13), 4969-4976.
7. Landmann, M.; Rauls, E.; Schmidt, W., The electronic structure and optical response of rutile, anatase and brookite TiO_2. *Journal of Physics: Condensed Matter* **2012,** *24* (19), 195503.

8. Cotton, F. A.; Wilkinson, G., *Advanced inorganic chemistry: a comprehensive text*. Interscience Publishers New York: 1972; Vol. 511.

9. Gonzalez, M. A.; Howell, S. G.; Sikdar, S. K., Photocatalytic selective oxidation of hydrocarbons in the aqueous phase. *Journal of Catalysis* **1999,** *183* (1), 159-162.

10. Carp, O.; Huisman, C. L.; Reller, A., Photoinduced reactivity of titanium dioxide. *Progress in Solid State Chemistry* **2004,** *32* (1), 33-177.

11. McKelvey, J. P., Solid State and Semiconductor Physics, Happer and Row,; New York.

12. Mori, K., Photo-functionalized materials using nanoparticles: photocatalysis,; nihon, s. f. R. D. c. c. r. l.; parkerizing. KONA, 23, 205-214.

13. Joshi, K.; Shrivastava, V., Photocatalytic degradation of Chromium (VI) from wastewater using nanomaterials like TiO_2, ZnO, and CdS. *Applied Nanoscience* **2011,** *1* (3), 147-155.

14. Herrmann, J.-M., Heterogeneous photocatalysis: fundamentals and; applications to the removal of various types of aqueous pollutants; Catal. Today, 53, 115–129.

15. Hodnett, B. K., *Heterogeneous catalytic oxidation: fundamental and technological aspects of the selective and total oxidation of organic compounds*. John Wiley: 2000.

16. Teoh, W. Y.; Mädler, L.; Beydoun, D.; Pratsinis, S. E.; Amal, R., Direct (one-step) synthesis of TiO_2 and Pt/ TiO_2 nanoparticles for photocatalytic mineralisation of sucrose. *Chemical engineering science* **2005,** *60* (21), 5852-5861.

17. Zhao, J.; Yang, X., Photocatalytic oxidation for indoor air purification: a literature review. *Building and Environment* **2003,** *38* (5), 645-654.

18. Herrmann, J.-M., Heterogeneous photocatalysis: fundamentals and applications to the removal of various types of aqueous pollutants. *Catalysis today* **1999,** *53* (1), 115-129.

19. Chen, D.; Ray, A. K., Photocatalytic kinetics of phenol and its derivatives over UV irradiated TiO_2. *Applied Catalysis B: Environmental* **1999,** *23* (2), 143-157.

20. Getoff, N., Factors influencing the efficiency of radiation-induced degradation of water pollutants. *Radiation Physics and Chemistry* **2002,** *65* (4), 437-446.

21. Palmisano, L.; Augugliaro, V.; Schiavello, M.; Sclafani, A., Influence of acid-base properties on photocatalytic and photochemical processes. *Journal of molecular catalysis* **1989,** *56* (1), 284-295.

22. Venkatachalam, N.; Palanichamy, M.; Murugesan, V., Sol–gel preparation and characterization of nanosize TiO_2: Its photocatalytic performance. *Materials Chemistry and Physics* **2007,** *104* (2), 454-459.

23. Bouras, P.; Stathatos, E.; Lianos, P., Pure versus metal-ion-doped nanocrystalline titania for photocatalysis. *Applied Catalysis B: Environmental* **2007,** *73* (1), 51-59.

24. Nolan, N. T., Sol-Gel Synthesis and Characterisation of Novel Metal Oxide Nanomaterials for Photocatalytic Applications. *Unpublished doctoral dissertation, Dublin Institute of Technology, Dublin, Ireland* **2010**.

25. Kuo, Y.-L.; Chen, H.-W.; Ku, Y., Analysis of silver particles incorporated on TiO_2 coatings for the photodecomposition of o-cresol. *Thin Solid Films* **2007,** *515* (7), 3461-3468.

26. Irie, H.; Watanabe, Y.; Hashimoto, K., Nitrogen-concentration dependence on photocatalytic activity of TiO_2-x Nx powders. *The Journal of Physical Chemistry B* **2003,** *107* (23), 5483-5486.

27. Ihara, T.; Miyoshi, M.; Iriyama, Y.; Matsumoto, O.; Sugihara, S., Visible-light-active titanium oxide photocatalyst realized by an oxygen-deficient structure and by nitrogen doping. *Applied Catalysis B: Environmental* **2003,** *42* (4), 403-409.

28. Martyanov, I. N.; Uma, S.; Rodrigues, S.; Klabunde, K. J., Structural defects cause TiO_2-based photocatalysts to be active in visible light. *Chemical communications* **2004,** (21), 2476-2477.

29. Nakamura, R.; Tanaka, T.; Nakato, Y., Mechanism for visible light responses in anodic photocurrents at N-doped TiO_2 film electrodes. *The Journal of Physical Chemistry B* **2004,** *108* (30), 10617-10620.

30. Asahi, R.; Morikawa, T.; Ohwaki, T.; Aoki, K.; Taga, Y., Visible-light photocatalysis in nitrogen-doped titanium oxides. *Science* **2001,** *293* (5528), 269-271.

31. Hamal, D. B.; Klabunde, K. J., Synthesis, characterization, and visible light activity of new nanoparticle photocatalysts based on silver, carbon, and sulfur-doped TiO_2. *Journal of colloid and interface science* **2007,** *311* (2), 514-522.

32. Barakat, M.; Schaeffer, H.; Hayes, G.; Ismat-Shah, S., Photocatalytic degradation of 2-chlorophenol by Co-doped TiO_2 nanoparticles. *Applied Catalysis B: Environmental* **2005,** *57* (1), 23-30.

33. Choi, W.; Termin, A.; Hoffmann, M. R., The role of metal ion dopants in quantum-sized TiO_2: correlation between photoreactivity and charge carrier recombination dynamics. *The Journal of Physical Chemistry* **1994,** *98* (51), 13669-13679.

34. Kang, M., The superhydrophilicity of Al– TiO_2 nanometer sized material synthesized using a solvothermal method. *Materials Letters* **2005,** *59* (24), 3122-3127.

35. Livage, J.; Sanchez, C., Sol-gel chemistry. *Journal of Non-Crystalline Solids* **1992,** *145*, 11-19.

36. Bach, S.; Henry, M.; Baffier, N.; Livage, J., Sol-gel synthesis of manganese oxides. *Journal of Solid State Chemistry* **1990,** *88* (2), 325-333.

37. Brinker, C. J.; Scherer, G. W., *Sol-gel science: the physics and chemistry of sol-gel processing*. Academic Pr: 1990.

38. Sanchez, C.; Livage, J.; Henry, M.; Babonneau, F., Chemical modification of alkoxide precursors. *Journal of Non-Crystalline Solids* **1988,** *100* (1), 65-76.

39. Yoldas, B. E., Alumina gels that form porous transparent Al_2O_3. *Journal of Materials Science* **1975,** *10* (11), 1856-1860.

40. Doeuff, S.; Henry, M.; Sanchez, C.; Livage, J., Hydrolysis of titanium alkoxides: modification of the molecular precursor by acetic acid. *Journal of Non-Crystalline Solids* **1987,** *89* (1), 206-216.

41. Zeleňák, V.; Vargová, Z.; Györyová, K., Correlation of infrared spectra of zinc (II) carboxylates with their structures. *Spectrochimica Acta Part A: Molecular and Biomolecular Spectroscopy* **2007,** *66* (2), 262-272.

42. Ivanda, M.; Furić, K.; Musić, S.; Ristić, M.; Gotić, M.; Ristić, D.; Tonejc, A.; Djerdj, I.; Mattarelli, M.; Montagna, M., Low wavenumber Raman scattering of nanoparticles and nanocomposite materials. *Journal of Raman Spectroscopy* **2007,** *38* (6), 647-659.

43. Nakamoto, K., *Infrared and Raman spectra of inorganic and coordination compounds*. Wiley Online Library: 1978.

44. Nara, M.; Tasumi, M.; Tanokura, M.; Hiraoki, T.; Yazawa, M.; Tsutsumi, A., Infrared studies of interaction between metal ions and Ca^{2+} binding proteins Marker bands for identifying the types of coordination of the side-chain COO^- groups to metal ions in pike parvalbumin (pI= 4.10). *FEBS letters* **1994,** *349* (1), 84-88.

45. Chen, X.; Liu, L.; Peter, Y. Y.; Mao, S. S., Increasing solar absorption for photocatalysis with black hydrogenated titanium dioxide nanocrystals. *science* **2011,** *331* (6018), 746-750.

46. (a) Kongsuebchart, W.; Praserthdam, P.; Panpranot, J.; Sirisuk, A.; Supphasrirongjaroen, P.; Satayaprasert, C., Effect of crystallite size on the surface defect of nano-TiO_2 prepared via solvothermal synthesis. *Journal of crystal growth* **2006,** *297* (1), 234-238; (b) Wu, X.; Jiang, Q.-Z.; Ma, Z.-F.; Fu, M.; Shangguan, W.-F., Synthesis of titania nanotubes by microwave irradiation. *Solid state communications* **2005,** *136* (9), 513-517.

47. Wu, L.; Yu, J. C.; Wang, X.; Zhang, L.; Yu, J., Characterization of mesoporous nanocrystalline TiO_2 photocatalysts synthesized via a sol-solvothermal process at a low temperature. *Journal of Solid State Chemistry* **2005,** *178* (1), 321-328.

48. Sakthivel, S.; Shankar, M.; Palanichamy, M.; Arabindoo, B.; Bahnemann, D.; Murugesan, V., Enhancement of photocatalytic activity by metal deposition: characterisation and photonic efficiency of Pt, Au and Pd deposited on TiO_2 catalyst. *Water Research* **2004,** *38* (13), 3001-3008.

49. Muggli, D. S.; McCue, J. T.; Falconer, J. L., Mechanism of the Photocatalytic Oxidation of Ethanol on TiO_2. *Journal of Catalysis* **1998,** *173* (2), 470-483.

50. Hashimoto, K.; Irie, H.; Fujishima, A., TiO_2 Photocatalysis: A Historical Overview and Future Prospects. *Japanese Journal of Applied Physics Part 1 Regular Papers Short Notes and Review Papers* **2005,** *44* (12), 8269.

51. Kudo, A.; Miseki, Y., Heterogeneous photocatalyst materials for water splitting. *Chemical Society Reviews* **2009,** *38* (1), 253-278.

52. Kato, N.; Higuchi, K.; Tanaka, H.; Nakajima, J.; Sano, T.; Toyoda, T., Improvement in long-term stability of dye-sensitized solar cell for outdoor use. *Solar Energy Materials and Solar Cells* **2011,** *95* (1), 301-305.

53. http://www.solarisnano.com/images/handheldcell.png. (22 June 2013)

54. http://photochemistryportal.net/home/index.php/tag/dye-sensitized-solar-cells/. (22 June 2013)

55. Pagliaro, M.; Palmisano, G.; Ciriminna, R.; Loddo, V., Nanochemistry aspects of titania in dye-sensitized solar cells. *Energy Environ. Sci.* **2009,** *2* (8), 838-844.

56. Sato, S.; Oimatsu, S.; Takahashi, R., Pore size regulation of TiO_2 by use of a complex of titanium tetraisopropoxide and stearic acid. *Chemical Communications* **1997,** (22), 2219-2220.

57. Takenaka, S.; Takahashi, R.; Sato, S.; Sodesawa, T., Structural study of mesoporous titania prepared from titanium alkoxide and carboxylic acids. *Journal of Sol-Gel Science and Technology* **2000,** *19* (1), 711-714.

58. Bessekhouad, Y.; Robert, D.; Weber, J., Preparation of TiO_2 nanoparticles by Sol-Gel route. *International Journal of Photoenergy* **2003,** *5* (3), 153-158.

59. Kolen'ko, Y. V.; Burukhin, A. A.; Churagulov, B. R.; Oleynikov, N. N., Synthesis of nanocrystalline TiO_2 powders from aqueous $TiOSO_4$ solutions under hydrothermal conditions. *Materials Letters* **2003,** *57* (5), 1124-1129.

60. Su, C.; Hong, B.-Y.; Tseng, C.-M., Sol–gel preparation and photocatalysis of titanium dioxide. *Catalysis Today* **2004,** *96* (3), 119-126.

61. Yang, H.; Zhang, K.; Shi, R.; Li, X.; Dong, X.; Yu, Y., Sol–gel synthesis of TiO_2 nanoparticles and photocatalytic degradation of methyl orange in aqueous TiO_2 suspensions. *Journal of Alloys and Compounds* **2006,** *413* (1), 302-306.

62. Wahi, R. K.; Liu, Y.; Falkner, J. C.; Colvin, V. L., Solvothermal synthesis and characterization of anatase TiO_2 nanocrystals with ultrahigh surface area. *Journal of colloid and interface science* **2006,** *302* (2), 530-536.

63. Sakthivel, S.; Hidalgo, M.; Bahnemann, D.; Geissen, S. U.; Murugesan, V.; Vogelpohl, A., A fine route to tune the photocatalytic activity of TiO_2. *Applied Catalysis B: Environmental* **2006,** *63* (1), 31-40.

64. Tian, C.; Zhang, Z.; Hou, J.; Luo, N., Surfactant/co-polymer template hydrothermal synthesis of thermally stable, mesoporous TiO_2 from $TiOSO_4$. *Materials Letters* **2008,** *62* (1), 77-80.

65. Štengl, V.; Houšková, V.; Murafa, N.; Bakardjieva, S., Synthesis of mesoporous titania by homogeneous hydrolysis of titania oxo-sulfate in the presence of cationic and anionic surfactants. *Ceramics-Silikáty* **2010,** *54* (4), 368-378.

66. Sharabi, D.; Paz, Y., Preferential photodegradation of contaminants by molecular imprinting on titanium dioxide. *Applied Catalysis B: Environmental* **2010,** *95* (1), 169-178.

67. Kraeutler, B.; Bard, A. J., Heterogeneous photocatalytic decomposition of saturated carboxylic acids on titanium dioxide powder. Decarboxylative route to alkanes. *Journal of the American Chemical Society* **1978,** *100* (19), 5985-5992.

68. Houas, A.; Lachheb, H.; Ksibi, M.; Elaloui, E.; Guillard, C.; Herrmann, J. M., Photocatalytic degradation pathway of methylene blue in water. *Applied Catalysis B: Environmental* **2001,** *31* (2), 145-157.

69. Konstantinou, I. K.; Sakellarides, T. M.; Sakkas, V. A.; Albanis, T. A., Photocatalytic degradation of selected s-triazine herbicides and organophosphorus insecticides over aqueous TiO_2 suspensions. *Environmental science & technology* **2001,** *35* (2), 398-405.

70. Qu, Q.; Geng, H.; Peng, R.; Cui, Q.; Gu, X.; Li, F.; Wang, M., Chemically Binding Carboxylic Acids onto TiO_2 Nanoparticles with Adjustable Coverage by Solvothermal Strategy. *Langmuir* **2010,** *26* (12), 9539-9546.